Simultaneously reinforce and de-color nanocellulose/lignin composite films by tuning hydroxyl groups with sodium borohydride

X. G. Liu [a], S. Y. Zeng [b], Q. F. Wang [c], J. Li [a,*], X. Tong [a,d], J. B. Chen [e], D. L. Guo [a], H. F. Zhao [a], X. H. Chen [a]

[a] *School of Environmental and Natural Resources, Zhejiang University of Science and Technology, Hangzhou 310023, China*

[b] *Jiangsu Co-Innovation Center of Efficient Processing and Utilization of Forest Resources, International Innovation Center for Forest Chemicals and Materials, College of Materials Science and Engineering, Nanjing Forestry University, Nanjing 210037, China*

[c] *Hangzhou Weipack Technology Co., Ltd, Hangzhou 310018, China*

[d] *Tianjin Key Laboratory of Pulp & Paper, Tianjin University of Science & Technology, Tianjin 300457, China*

[e] *Winbon Schoeller New Materials Co., Ltd., Quzhou 324400, China*

Researchers utilized $NaBH_4$ to gently modify alkali lignin, resulting in L-S_x-t_y-P_z with high hydroxyl value and decolorization, significantly enhancing the strength of composite films with cellulose nanofibers (CNF). Without strict pH control, the hydroxyl content of the modified lignin reached as high as 9.14 mmol/g. The CF/L-S_1-t_{120}-P_u composite film achieved a maximum stress of 45.33 MPa, representing a 116% and 77% increase compared to pure CNF and crude alkali lignin composite films, respectively. The reduction effect of $NaBH_4$ imparted transparency to the film, broadening its applications. Additionally, the film's excellent antibacterial and flame-retardant properties provide strong support for industrial utilization.

(Received October 22, 2024; Accepted January 9, 2025)

Keywords: Lignin, $NaBH_4$, Hydroxyl groups, Composite film, Multi-functional properties

1. Introduction

Lignin, as the most abundant aromatic compound in nature, has been widely used in the fields of active packaging [1], due to its antimicrobial [2], UV-resistant [3], and fire-retardant properties [4]. Based on the various characters, lignin has been composited with diverse forms in degradable bio-based films including cellulose nanofibers (CNF) [5 6], starch [7], and polyvinyl alcohol (PVA) [8] in numerous historical studies. Nevertheless, due to the intrinsic heterogeneity of lignin, the fabrication of hybrid films whose mechanical strength could be comparable to traditional plastic films still encountered many challenges.

* Corresponding author: jingli@zust.edu.cn

https://doi.org/10.15251/DJNB.2025.201.23

Inspired by the lignin-cellulose network in natural wood, various fabrication methods were investigated aiming to build tense hydrogen bonding network among the composited agents [9-13]. Regeneration of dense network featuring the interior nanoscale entanglement and hydrogen bonding treated by the mild deep eutectic solvent was once suggested, and the resulted bio-plastics exhibited high mechanical strength, excellent water stability, ultraviolet-light resistance and improved thermal stability [14]. Nano-fabrication strategies representing that lignin nanoparticles, lignin nanospheres, and lignin nano-rod was regulated to obtain lower molecular weight, higher phenolic hydroxyl group content, and uniform morphology were successfully prepared as reinforcing agent [15]. Some scholars extracted lignin by solvents such as acetone, methanol, ethanol, and ethyl acetate, and prepared composite membranes from the extracted lignin with CNF and starch, verifying the effects of different -OH contents in lignin on the strength of composite membranes, and also using small molecular weight lignin as a compatibilizer of starch and CNF in composite membranes, thus improving the integrity and mechanical properties of composite membranes. However, the lignin addition had a negative effect on the thermal stability of the composite membrane as the residual weight (char) of the membrane at 800 °C was only 10.3% [16]. In order to address the thermal stability of composite membranes, lignocellulosic nanofibrils (LCNF) suspension containing 0.1, 3.9, and 17.2 wt% lignin were utilized to fabricate films by filtration and pressing process. The maximum weight loss temperature (T_{max}) was 372 °C, which improved the thermal stability performance of the composite membrane, but the inhomogeneity of the membrane surface structure led to the elevation of the membrane surface roughness value, and the lignin in the membrane interfered with the hydrogen bonding between the LCNF, which impaired the mechanical properties of the membrane [17].After phenolated by phenol in acid conditions, lignin nanoparticles were prepared by solvent-antisolvent method and the resulted phenolic hydroxyl group content achieved as high as 8.23 mmol/g. CNFs mixed with phenolated LNPs of high Ph-OH content (8.23 mmol/g) exhibited a higher tensile strength (~190 MPa), increased toughness (~15 MJ/m3), and enhanced UV-blocking ability (~99 %) [9]. Based on this, crosslinking with chemical compound (i.e. tannic acid) possessing abundant hydroxyl groups could also assist and boost the enhancement of the mechanical strength. Lignin nanoparticles loaded with potassium sorbate (LNP@PS) were firstly prepared, and then tannic acid (TA) and PVA were added to prepare composite films, which led to a substantial increase in the tensile strength of the composite film as well as water vapor, etc. The optimal tensile strength of the PVA-based composite film with 3 % LNP@PS and 5 % TA was 74.51 MPa, and the water vapor permeability was $7.015 \cdot 10^{-13}$ g cm/cm^2 s Pa, and an oxygen transmission rate of 1.93 cm^3/m^2 24hMPa [18 19]. Besides, lignin was also employed as functional filler to endow the composite films with versatile barrier and mechanical properties [20 21]. By modifying lignin, the strength, UV resistance and other properties of lignin-based composite films are well improved, but the modification does not affect the original color of lignin, which makes the chromaticity of the prepared composite film larger, and therefore may limit its wide application.

In this paper, a novel method based on the strongly reductive and selective properties of $NaBH_4$ was proposed to modify AL under mild conditions, aiming at tuning the interior hydroxyl groups to build more hydrogen bonds with cellulose nanofibers and achieve the de-coloring results. Meanwhile, the morphology, physical strength, thermal stability and properties of UV shielding of the composite films were also analyzed as shown in Fig. 1.

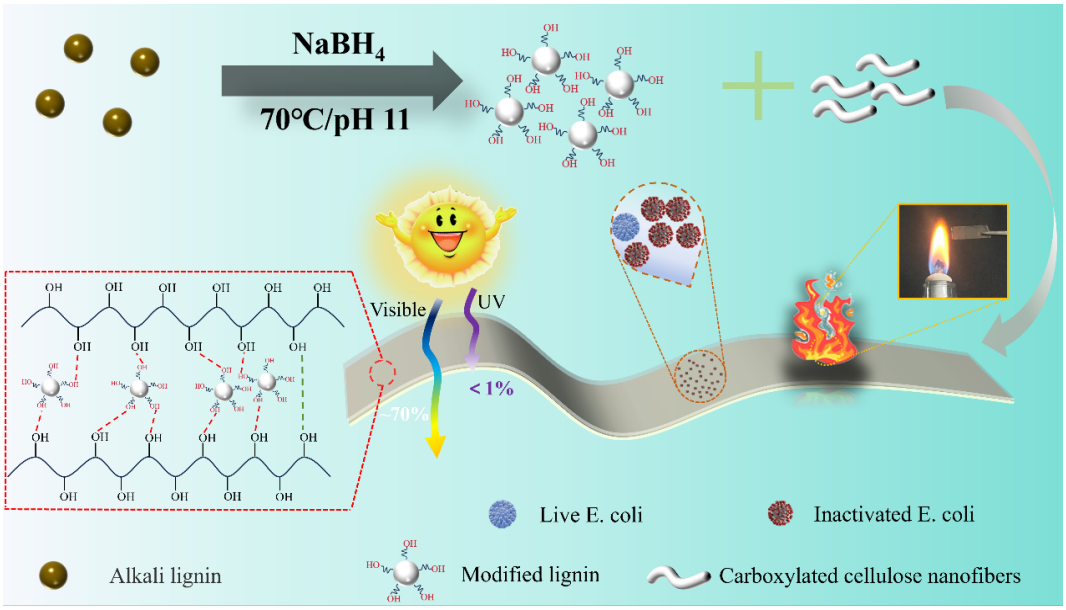

Fig. 1. Mechanism of composite film preparation.

2. Materials and methods

2.1. Materials

Carboxylated cellulose nanofibers (CNF, average diameter: 50 nm, length: 1-3 μm), alkaline lignin (AL, average Mw: 500), and Sodium borohydride ($NaBH_4$) were all purchased from Macklin Reagent (Shanghai) Co. Ltd without any further treatment.

2.2. Lignin modification

$NaBH_4$ was employed to prepare the modified lignin (ML). In detail, 1g, 2g of $NaBH_4$ to selectively reduce 1g of lignin in 10 mL of deionized water under 70°C for 30min, 60min, and 120min at pH 11 or uncontrollable pH, and then vacuum dried at 60°C until totally dried. The resulting modified lignin samples were denoted as L-S_x-t_y-p_z, where x represented the dosage of $NaBH_4$, y represented the reduction process time, and z represented pH at 11 or uncontrol. For example, L-S_1-t_{30}-p_u meant that 1 g of $NaBH_4$ was used to reduce 1 g of lignin in 10 mL of deionized water under 70°C for 30min at uncontrollable pH.

2.3. Preparation of composites films

3wt % CNF solution was prepared firstly by dissolving CNF in deionized water and stirred for 2 h, and then certain amounts of ML was added to prepare mixed solution containing 10wt% ML, which was then stirred for another 1h to ensure thorough mixing. Following, the mixtures were immediately poured into polytetrafluoroethylene molds and then dried slowly at room temperature to get composite films (CF) with different L-S_x-t_y-p_z, i.e. CF/L-S_x-t_y-p_z.

2.4. Characterization

2.4.1. Hydroxyl content

Accurately weigh 30 mg of lignin in beaker and add 5 mL of 1 mol/L potassium hydroxide solution and 50 mg of hydroxybenzoic acid as internal standard. After adding 50 mL of ultrapure water, the lignin and internal standard were fully dissolved, and the titration experiment was carried out with hydrochloric acid as the titrant to obtain the first grade microquotient curve. Another 5 mL of 1 mol/L potassium hydroxide solution and 50 mg of internal standard hydroxybenzoic acid were placed in a beaker and 50 mL of ultrapure water was added to ultrasonically dissolve the lignin and the internal standard, and then the titration experiment was carried out as a blank control. Each group of experiments was repeated three times.

2.4.2. Chemical properties

Fourier transform infrared spectroscopy (FT-IR, 8400 S, Shimadzu, Kyoto, Japan) analysis was carried out for the functional groups in CF/L-S_x-t_y-p_z samples.

2.4.3. Micro-morphological characterization/ energy X-ray dispersion spectroscopy (EDS)

The surface morphology and micro-structure of AL and composite films were observed using scanning electron microscope (SEM, S3400, Hitachi, Tokyo, Japan) with accelerating voltage of 15 KV.

2.4.4. Mechanical strength

A universal tensile machine (KYD-2000NS, Tiandu Technology, ZheJiang, China) was used to measure the mechanical properties of the composite film material, including the tensile strength and strain curve. Plastic tensile property mark mechanical property test refer to the ASTM-D638 standard test method, before the mechanical test, the samples were pre-conditioned indoors for 1 week at 50% relative humidity and 23 ℃, the specimens were preloaded with a force of 5 N to eliminate the relaxation, and the composite film was cut into a rectangular strip with a length of 50 mm and a width of 10 mm, and the tensile rate was set to 5 mm/min, and each sample was tested for 3 times, and the results were averaged.

2.4.5. Thermal properties

Thermal analysis was carried out using a Synchronized Thermogravimetric Analyzer (TGA, Seiko Extra 6300, Kyoto, Japan) equipment. In this study, nitrogen atmosphere was tested at a gas flow rate of 100 ml min^{-1}. Analyses were carried out between 40 and 600 °C with a heating rate of 10 °C min^{-1}. The maximum decomposition temperature was determined from a first order derivative thermogravimetric analysis curve (DTG).

2.4.6. UV-visible spectral analysis

The visible light transmittance of the films was measured using a UV-visible spectrophotometer (Shimadzu UV-2600 spectrometer, Japan). The transmittance was recorded at 200-800 nm. The film specimens were cut into 30 mm-10 mm rectangles and placed in 10 mm quartz test tubes. The instrument was equipped with a kinetic mode of operation to record the complete spectrum continuously at a frequency of every 10 s.

2.4.7. Optical properties

The films were firstly cut into rectangles (10 × 40 mm^2) and placed in a quartz cuvette. Referred to air, the spectrometer within the range of 200-800nm were recorded using Shimadzu UV-2600 with three times [16]. The Opacity (Op) was calculated using Eq. (1)

$$Opacity = \frac{A_{600}}{d} \quad (1)$$

where A_{600} was the absorbance value measured at 600 nm, and *d* was the thickness of the film.

2.4.8. Antimicrobial properties

Referring to the method [22] and improving it appropriately, the prepared Escherichia coli(*E.coli*)suspension was uniformly applied on the cooled and solidified agar medium, and the modified lignin composite film was cut off by punching holes with a 5mm sterile punch, and the cut composite films were placed in the center of the agar medium, and each group of composite films was subjected to three groups of parallel tests, and placed in a 37 ℃ constant temperature incubator for 24 h. The antibacterial performance of the material was judged according to the size of the inhibition circle.

2.4.9. Flame retardancy analysis/LOI

The composite film was cut into strips with width of 10 mm for the combustion experiment which was carried out for a period of 15 s from the beginning of the material contacting the flame. The sample is cut into strips of 1 × 5 cm^2 and placed vertically in the limiting oxygen index tester. A flame source of about 12 mm in width is introduced from the outside to contact the upper edge of the sample, and it is ensured that the sample begins to burn without stopping by itself. The oxygen concentration of the sample when burning for 180 s is measured, which is the limiting oxygen index concentration of the material.

3. Results and discussion

3.1. Hydroxyl content in lignin

Hydroxyl groups in lignin was considered as the basis to form hydrogen bonds which was the main bonding forces to maintain the mechanical strength in composite films. Historically reported demethylation methods using 1-dodecanethiol (DSH) [23], there will also be phenolic modification with phenol is also performed[9] or hydroxylation modification of purified enzymatic lignin with H_2O_2 and $Fe(OH)_3$ [24] were usually employed to obtain hydroxyl groups aiming at constructing more hydrogen bonds and strengthening the films. In this study, $NaBH_4$ was used as an excellent selective reducing agent to modulate the hydroxyl groups in AL. Based on the strong reducing property of NaBH4, during the reaction process, the hydrogen-negative ions (H^-) in $NaBH_4$ attacked the carbonyl carbon atoms to form a carbon-negative intermediate, which subsequently interacted with water molecules to generate hydroxyl groups or reduced the carbonyl groups attached to the benzene ring to phenol, resulting in the enhancement of the modified AL hydroxyl group(-OH) content. It also showed stronger reducing activity in alkaline environment, where it

reacted with the carbonyl group (C=O) in alkali lignin and reduced it to -OH. As shown in Table 1, the total hydroxyl content in L-S_1-t_{120}-P_u and L-S_1-t_{60}-P_{11} increased by 6.36 mmol/g and 4.88 mmol/g, compared with that of crude lignin sample of 2.78 mmol/g.

Table 1. Comparison of hydroxyl content from different lignin samples.

Lignin samples	Hydroxyl content/(mmol/g)	Reference
Kraft lignin	4.33	9
Phenolated Kraft lignin	6.63	
DSH demethylated lignin	5.69	22
Enzymatic hydrolysis lignin (EHL)	3.11	23
Hydroxylated EHL	4.16	
Crude alkaline lignin	2.78	This work
L-S_1-t_{120}-P_u	9.14	
L-S_1-t_{60}-P_{11}	7.66	

3.2. Composite films

3.2.1. Physical properties

Table 2 showed CF-AL, CF/L-S_1-t_{30}-P_u, CF/L-S_1-t_{120}-P_u, CF/L-S_1-t_{60}-$P_{11}$the thickness and opacity values of the composite and CNF films. The thickness of the CNF film was 0.113 mm, and with the addition of crude and modified lignin, the thickness of the composite films increased a lot, since the added lignin particles suppressed the aggregation of cellulose nanofibrils. Some scholars cellulose nanofibers (CNF) and cellulose nanocrystals (CNC) prepared nanocomposite films with opacity ranging from 16.0 to 7.3 [25]. Due to the strongly reductive effect from $NaBH_4$ on the chromogenic groups in lignin, i.e. carbonyl groups and ketone groups, the opacity results of the composite films with modified lignin exhibited an apparent decrease from 8.703 to 7.304, which was almost similar to the pure CNF films.

Table 2. Physical properties of modified composite and CNF films.

Samples	Thickness (mm)	Opacity
CNF	0.113	7.142
CF@AL	0.118	8.703
CF/L-S_1-t_{30}-P_u	0.121	7.708
CF/L-S_1-t_{60}-P_u	0.121	7.554
CF/L-S_1-t_{120}-P_u	0.122	7.304
CF/L-S_1-t_{60}-P_{11}	0.122	7.304

Moreover, as shown in Fig. 3 a, the pure CNF film was smooth, bright and transparent. However, with the addition of the crude AL, the film appeared brown and lignin aggregation also existed in the interior of the film. Without controlling the modification process pH or controlling the pH under 11, the phenomenon of lignin aggregation disappeared with the extension of modification time, possibly because the modification assisted the more formation of hydroxyl groups, so that the negative charges in the carboxylated CNF could provide circumstances for dispersing lignin particles uniformly [26](Fig. 2), and therefore the composite films with modified lignin could be

comparative to the pure CNF films, which could also be proved by the opacity results in Table 2. From the micro-morphology of the films as shown in Fig. 3 (b-m), the uniform and dense structure was proved. With the incorporation of lignin, there was no obvious phase separation or lignin aggregation in the interior of the films, possibly because that with the modification processing, the higher amount of hydroxyl groups in lignin built more accesses to ensuring the connectivity between CNF and lignin, not only improving the dispersity of lignin particles, but also possibly enhancing the mechanical strength and toughness.

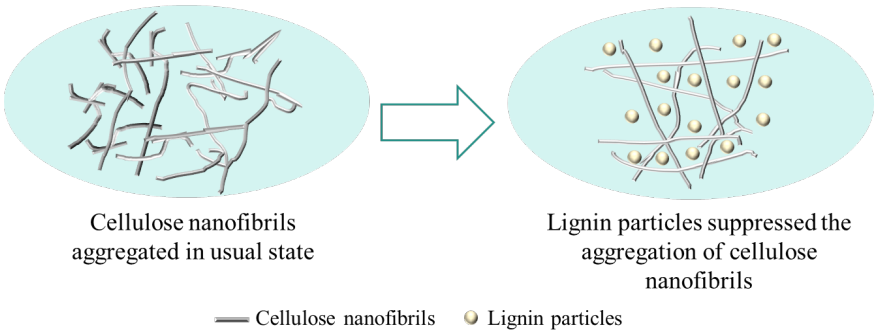

Fig. 2. Dispersion of lignin particles in CNF improved the uniform dispersion.

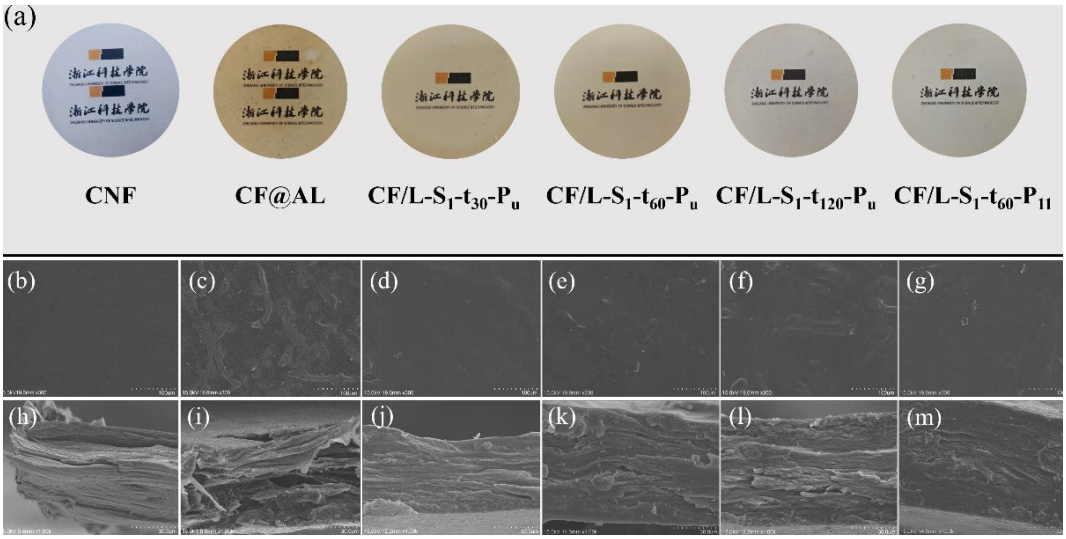

Fig. 3. (a) Photographs of different modified lignin composite and CNF films, (b-g) the surficial and (h-m) cross-section morphology of pure CNF, CF@-AL, CF/L-S_1-t_{30}-P_u, CF/L-S_1-t_{60}-P_u, CF/L-S_1-t_{120}-P_u, CF/L-S_1-t_{60}-P_{11}.

3.2.2. Strength properties

A study was conducted to prepare nanocomposite films from polylactic acid/polyaniline (PANI)/nanocrystalline cellulose (NCC), and the maximum tensile strength of the composite film was 26.1 MPa [27]. Graft modification with 3-aminopropyltriethoxysilane (KH-550) to improve the compatibility of PLA/NCC mixtures, PLA/NCC composite membranes were prepared by mixing with different ratios, with a maximum stress of 43.1 MPa and a maximum strain of 11% [28]. To

prove that the uniform dispersion of modified lignin particles and that the increased amount of hydroxyl group could reinforce the composite films, the stress-strain curves were obtained and shown in Fig. 4 a. As shown, the maximum stress of the CNF films was only 21.01 MPa. When AL was added, the strength of the CF@AL film was increased to 25.58 MPa, while the corresponding toughness had an apparent increase. With the addition of the modified lignin, the stress increased to 45.33 MPa for CF/L-S_1-t_{120}-P_u with the scarification of toughness to limited extent. With the addition of the modified lignin under pH 11 in CNF films, i.e., CF/L-S_1-t_{60}-P_{11}, the stress decreased about 10 MPa compared to the films with modified lignin under uncontrollable pH, possibly because the weakly alkaline environment promoted the ineffective consumption of $NaBH_4$.

Hydrogen bonding interactions between AL and CNF were characterised by FTIR (Fig. 4 b). The broad band at 3340cm^{-1} corresponds to the -OH stretching vibration frequency [29]. The -OH peak did not change after the addition of AL, when with the addition of L-S_1-t_{120}-P_u, the -OH peak of the CF/L-S_1-t_{120}-P_u composite film shifted forward to 3260 cm^{-1}, while the -OH peak of the composite film with the addition of L-S_1-t_{60}-P_{11} shifted forward to 3270 cm^{-1}. Upon addition of L-S_x-t_y-p_z, -OH shifted towards lower wave numbers, which is considered to be the formation of intermolecular hydrogen bonds between AL and CNFs.

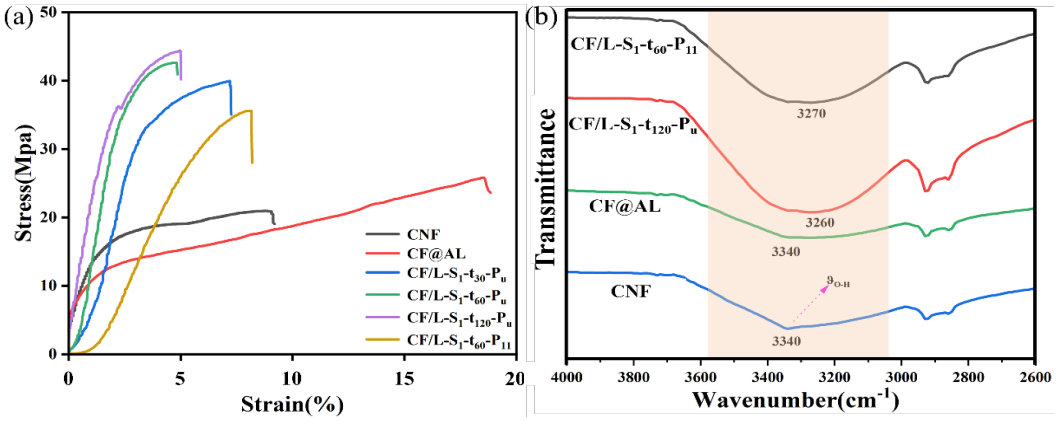

Fig. 4. (a) Stress-strain curves (b) FTIR spectra.

3.2.3. Anti-UV performance

It was known that lignin could provide ultra-violet shielding characteristic in various matrix-based on its aromatic structure, hydroxyl groups and carbonyl groups which were also chromogenic or auxochrome groups [18]. To verify the little effect of $NaBH_4$ reduction on anti-UV performance, the wavelength of 200-800 nm was chosen as shown in Fig. 5. The CF/L-S_1-t_{120}-P_u when modified with $NaBH_4$ for 120 min, and the film could block nearly 99% of UV light [30], at the same time, the visible light transmission can be greatly improved. The UV-absorbing properties of the composite film can be used for materials designed for outdoor exposure or for packaging of photosensitive products.

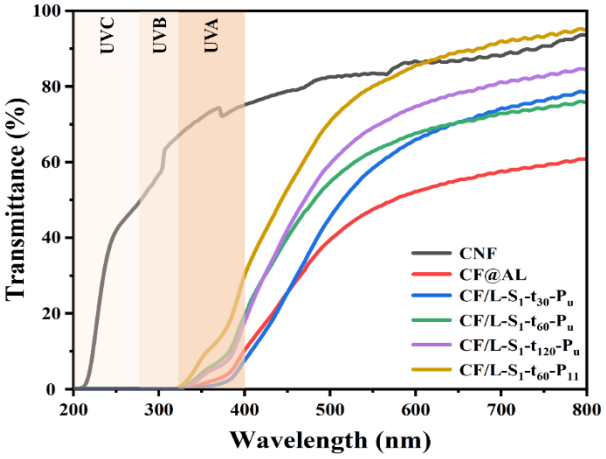

Fig. 5. UV shielding properties of CNF-based composites films.

3.2.4 Antimicrobial performance

The antibacterial circle was usually used to reflect the antibacterial performance of the films, when the composite films diffuse in the agar plate so that the bacterial growth around it is inhibited and a transparent circle is formed, the larger the range of the antibacterial circle indicates the stronger the antibacterial performance. It can be seen that the pure CNF film still maintained the original state after 24h of cultivation (Fig. 6 e), and did not produce the bacterial inhibition circle, which indicated that the pure CNF film had no bacterial inhibition activity against E. coli. The CF@AL composite film showed a 0.5 mm wide area without bacterial growth after 24 h, indicating that the CF@AL composite film began to gradually produce antibacterial activity against E. coli after 24 h (Fig. 6 f). While CF/L-S_1-t_{60}-P_{11} and CF/L-S_1-$t1_{20}$-P_u composite films showed 2 mm wide antibacterial effect around the films after 12 h of incubation, compared with the antimicrobial properties of CF@AL composite film, the release of bacterial inhibitory properties in a shorter period of time and continued to act in 24h, the composite film modified by $NaBH_4$ showed excellent antimicrobial properties, it may be due to the high content of phenolic hydroxyl groups that can disrupt the bacterial cell wall more effectively and inhibit the growth and reproduction of bacteria. which provide an insight for the preparation of antimicrobial materials [22].

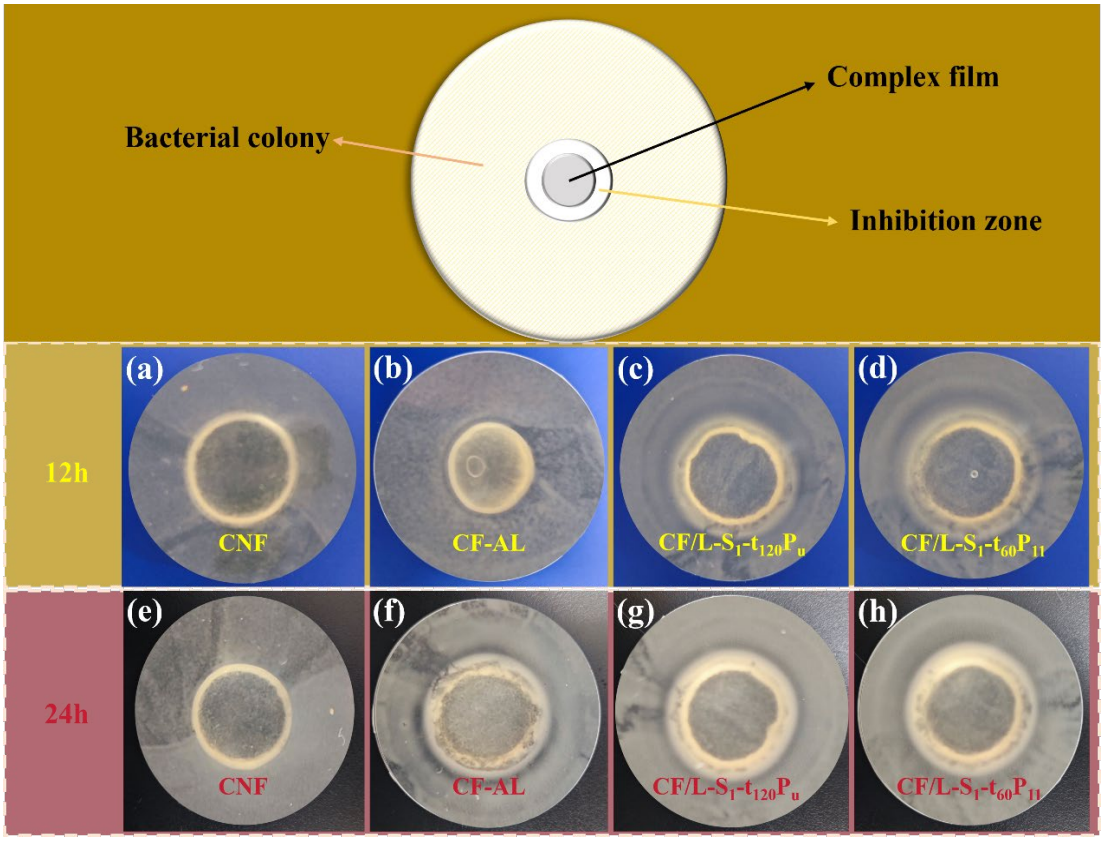

Fig. 6. Antibacterial physical diagram of different films.

3.2.5. Thermal and flame-retardant properties

Regarding the thermal stability of composite film [31], the weight loss of CNF and composite film mainly occurred at 200-600 °C (Fig. 7 a b). The thermal stability property of lignin is one of its major advantages, and the addition of lignin may positively affect the thermal stability of composite films. The TG curves of the CNF films show that the temperature of T_{min} is 251°C, while T_{max} only reaches 271°C. The degradation almost tends to equilibrate after 500°C. The small mass loss in the range of 75°C- 125°C is mainly caused by the loss of adsorbed bound water, and the largest mass loss between 250°C - 270°C is mainly the degradation of CNF itself, with the residual mass being only 28.3%. When a certain amount of AL was added, the adsorbed bound water was lost in volatilization at 40°C - 100°C due to the water absorption of AL, while there was a small degradation peak between 260°C - 270°C, which was due to the cleavage of organic matter in lignin, and the mass loss between 280°C - 320°C was mainly due to thermal decomposition of C=O [32]. When L-S_1-t_y-P_u was added, the overall degradation trend was the same as that of AL, but the thermal degradation peaks were all shifted to higher temperatures, which was based on the fact that the modification with $NaBH_4$ allowed the decomposition of the active functional groups, which resulted in a more stable thermal performance when complexed with CNF. Meanwhile the considerable stabilization of unsaturated aldehydes/ketones elevated the residual mass to 40% [33].

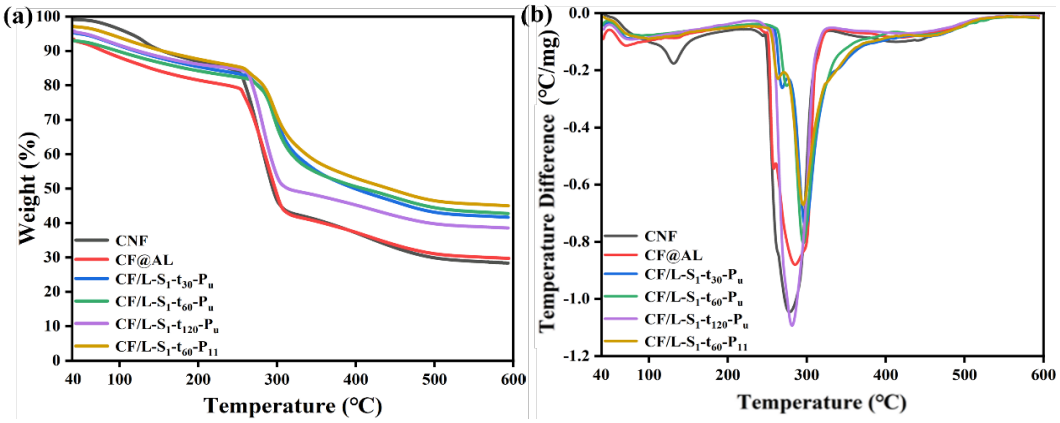

Fig. 7. (a) TG curves (b) DTG curves.

Following, direct flame ignition was used to characterize the actual flame-retardant performance and validate the effect from tuning hydroxyl groups. As shown in Fig. 8, the pure CNF film and CF@AL composite film started to burn immediately after contacting with flame and continued to burn within 15 s. On the other hand, CF/L-S_1-t_{60}-P_u and CF/L-S_1-t_{60}-P_{11} composite films do not burn immediately after contact with flame, but start to burn gradually after 15 s of contact with flame. The whole process of combustion of the composite film can be seen in the Fig. 10, and the composite film maintains its original material form after combustion, which indicates that the combustion caused by the cellulose component can be suppressed quickly and efficiently even in the case of continuous combustion [34]. By performing LOI tests on the composite film, the limiting oxygen index of CNF was 24.3%, and CF@AL with an added amount of AL only increased by 2.8%. When L-S_1-t_{120}-P_u was added, the limiting oxygen index of CF/L-S_1-t_{120}-P_u increased to 33.8%. By adding L-S_x-t_y-P_z, the flame-retardant property of the composite film is improved.

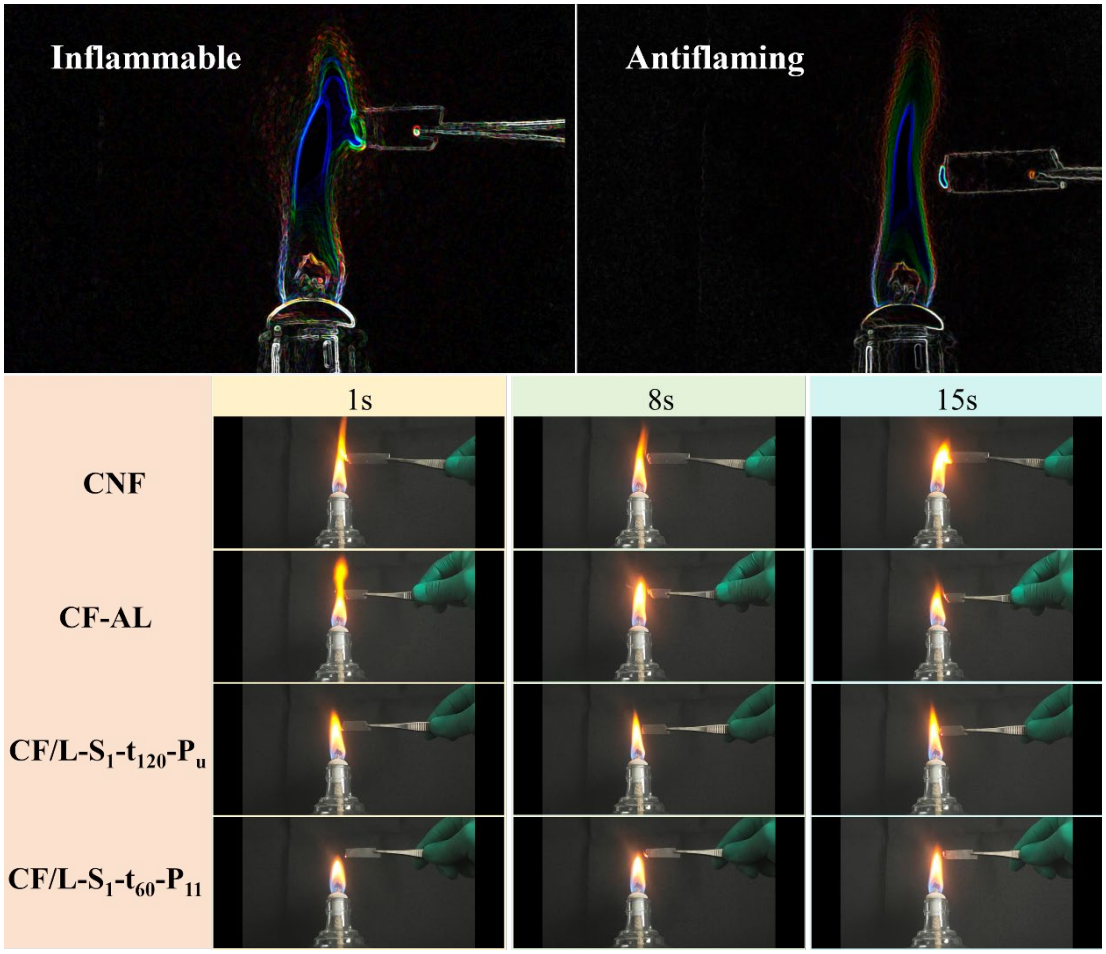

Fig. 8. Flame retardance performance of different films.

Table 3. Composite film limiting oxygen index.

Sample	LOI
CNF	24.3%
CF@AL	27.1%
CF/L-S_1-t_{120}-P_u	33.8%
CF/L-S_1-t_{60}-P_{11}	33.7%

4. Conclusion

In summary, the modification of AL with $NaBH_4$ at lower temperatures significantly increased the hydroxyl content in lignin, and the total hydroxyl content of L-S_1-t_{120}-P_u could reach 9.14 mmol/g, and the multifunctional composite film was successfully prepared. With the addition of modified lignin, the strength of the composite film was greatly improved, and the maximum tensile strength of CF/L-S_1-t_{120}-P_u could reach 45.33 MPa. Meanwhile, the transmittance of the composite film to visible light could reach more than 90%, and at the same time, the composite film maintained excellent UV-resistance, with UV transmittance <1%. In addition, the antimicrobial and flame-retardant properties of the composite film have been greatly improved. The composite film

still maintains excellent antimicrobial properties at 24 hours, and the limiting oxygen index of CF/L-S_1-t_{120}-P_u is 33.8%, which is an improvement of 39.1% compared with the pure CNF film. This makes the composite film a certain replacement in the field of food packaging as well as agricultural mulch.

Acknowledgements

The authors are thankful to the support of the "Pioneer" and "Leading Goose" R&D Program of Zhejiang (Grant No. 2023C01195), the Natural Science Foundation of Zhejiang Province (Grant No. LTGS23C160001), National Natural Science Foundation of China (Grant No.22308333), the Foundation (Grant No. 202202) of Tianjin Key Laboratory of Pulp & Paper, and the Fundamental Research Funds for Zhejiang University of Science and Technology (Grant No. 2023QN048, 2023JLZD006).

References

[1] Q. Q. Xia, C. J. Chen, Y. G. Yao, G. J. Li, S. M. He, Y. B. Zhou, T. Li, X. J. Pan, Y. Yao, L. B. Hu, Nat. Sustain. 4, 627-635 (2021); https://doi.org/10.1038/s41893-021-00702-w

[2] A. G. Morena, T. Tzanov, Royal Society of Chemistry publishes. 4, 4447-4469 (2022); https://doi.org/10.1039/D2NA00423B

[3]. X. Q. Li, J. Y. Li, X. Y. Shen, M. Y. Cao, Y. Wang, W. S. Zhang, Y. L. Xu, Z. Ling, S. Chen, F. Xu, ACS Sustainable Chemistry & Engineering. 12, 5427-5435 (2024); https://doi.org/10.1021/acssuschemeng.3c07076

[4] H. T. Yang, B. Yu, X. D. Xu, S. Bourbigot, H. Wang, P. G. Song, Green Chem. 22, 2129-2161 (2020); https://doi.org/10.1039/D0GC00449A

[5] R. Tian, C. Wang, W. K. Jiang, S. Janaswamy, G. H. Yang, X. X. Ji, Small. 22, 2309651 (2024).

[6] Y. Deng, Q. Q. Guan, L. He, L. C . Peng, J. H. Zhang, Carbohydr. Polym. 263, 117981 (2021); https://doi.org/10.1016/j.carbpol.2021.117981

[7] S. H. Wang, Hao, Y. L. He, Q. X. He, Q. Q. Gao, Thermoplast. Compos. Mater. 08927057241233566 (2024).

[8] T. Luo, C. Wang, X. X. Ji, G. H. Yang, J. C. Chen, C. G. Yoo, S. Janaswamy, G. J. Lyu, International Journal of Biological Macromolecules. 183, 781-789 (2021); https://doi.org/10.1016/j.ijbiomac.2021.05.005

[9] J. F. Ou, S. N. Hu, L. Yao, Y. Chen, H. S. Qi, F. X. Yue, Chemical Engineering Journal. 453, 139770 (2023); https://doi.org/10.1016/j.cej.2022.139770

[10] X. Z. Wang, Q. Q. Xia, S. S. Jing, C, Li, Q. Y. Chen, B. Chen, Z. Q. Pang, B. Jiang, W. T. Gan, G. Chen, M. J. Cui, L. B. Hu, T. Li, Small. 17, 2008011 (2021); https://doi.org/10.1002/smll.202008011

[11] B. Jiang, C.J. Chen, Z.Q. Liang, S. M. He, Y. D. Kuang, J. W. Song, R. Y. Mi, G. G. Chen, M. L. Jiao, L. B. Hu. Advanced Functional Materials. 30, 1906307 (2020); https://doi.org/10.1002/adfm.201906307

[12] M. Farooq, T. Zou, G. Riviere, M. H. Österberg Sipponen, M. Strong, Biomacromolecules 20, 693-704 (2019); https://doi.org/10.1021/acs.biomac.8b01364

[13] J. L. Wang, W. Chen, T. T. Dong, H. Q. Wang, S. R Si, X. S. Li Green Chem. 23, 10062-10070 (2021); https://doi.org/10.1039/D1GC03906G

[14] Z. Yuan, H. Liu, W. F. Yong, Q. She, J. Esteban, Green Chem. 24, 1895-1929 (2022); https://doi.org/10.1039/D1GC03851F

[15] Q. Q. Guan, J. J. Chen, D. Chen, X. S. Chai, L. He, L. C Peng, J. H. Zhang, J. Li, Journal of Catalysis. 370, 304-309 (2019); https://doi.org/10.1016/j.jcat.2019.01.003

[16] Y. Zhao, A. Tagami, G. Dobele, M. E. Lindström, O. Sevastyanova, Polymers 11, 538 (2019); https://doi.org/10.3390/polym11030538

[17] H. Y. Bian, Y. Gao, R. B. Wang, Z. L. Liu, W. B. Wu, H. Q. Dai, Cellulose. 25, 1309-1318 (2018); https://doi.org/10.1007/s10570-018-1658-x

[18] S. Y. Zeng, X. g. Liu, J. Li, H. f. Zhao, D. l. Guo, X. Tong, International Journal of Biological Macromolecules. 264, 130474 (2024); https://doi.org/10.1016/j.ijbiomac.2024.130474

[19] J. Li, H. C. Hu, X. S. Chai, AIChE Letter: Reaction Engineering, Kinetics and Catalysis. 63, 1489-1493 (2017); https://doi.org/10.1002/aic.15681

[20] S. Kirar, D. Mohne, M. Singh, V. Sagar, A. Bhise, S. Goswami, J. Bhaumik, Sustainable Materials and Technologies. 40, e00864 (2024); https://doi.org/10.1016/j.susmat.2024.e00864

[21] X.Q. Li, J. Y. Li, X. Y. Shen, M. Y. Cao, Y. Wang, W. S. Zhang, Y. L. Xu, L.S. Chen, F. Xu, X. Li, ACS Sustainable Chemistry & Engineering. 12, 5427-5435 (2024); https://doi.org/10.1021/acssuschemeng.3c07076

[22] A. K. Das, K. Mitra, A. J. Conte, A. Sarker, A. Chowdhury, A. J. Ragauskas, A. K. Das, International Journal of Biological Macromolecules. 261, 129753 (2024); https://doi.org/10.1016/j.ijbiomac.2024.129753

[23] K. Sawamura, Y. Tobimatsu, H. Kamitakahara, T. Takano, ACS Sustainable Chemistry & Engineering. 5, 5424-5431 (2017); https://doi.org/10.1021/acssuschemeng.7b00748

[24] T. Liu, Y. Wang, J. Zhou, M. Li, J. Yue, Polymers 13, 1349 (2021); https://doi.org/10.3390/polym13091349

[25] Y. Hua, T. Chen, Y. Tang, Industrial Crops and Products. 179, 114686 (2022); https://doi.org/10.1016/j.indcrop.2022.114686

[26] Y. X. Liu, ACS Sustainable Chemistry & Engineering. 6, 5524-5532 (2018); https://doi.org/10.1021/acssuschemeng.8b00402

[27] X. Wang, Y. Tang, X. Zhu, Y. Zhou, X. Hong, International Journal of Biological Macromolecules. 146, 1069-1075 (2020); https://doi.org/10.1016/j.ijbiomac.2019.09.233

[28] K. Jin, Y. Tang, X. Zhu, Y. Zhou, International Journal of Biological Macromolecules. 162, 1109-1117 (2020); https://doi.org/10.1016/j.ijbiomac.2020.06.201

[29] Figueiredo, P. P. Figueiredo, M. H. Lahtinen, M. B. Agustin, D.M. Carvalho, S.P. Hirvonen, P. A. Penttilä, ChemSusChem 14, 4718-4730 (2021); https://doi.org/10.1002/cssc.202101356

[30] H. Bian, H. Y. Bian, L. D. Chen, M. L. Dong, L. Y. Wang, R. B. Wang, X. L. Zhou, C. Wu, X. Wang, X. X. Ji, H. Q. Dai, International Journal of Biological Macromolecules. 166, 1578-1585 (2021); https://doi.org/10.1016/j.ijbiomac.2020.11.037

[31] S. S. Nair, N. Yan, Cellulose 22, 3137-3150 (2015); https://doi.org/10.1007/s10570-015-0737-5

[32] C. Li, J. H. Shi, Y. Y. Sun, L, J. Zhang, S. Zhang, S. Wang, X. Hu, Journal of Analytical and Applied Pyrolysis. 155, 105031 (2021); https://doi.org/10.1016/j.jaap.2021.105031

[33] Y. He, H. C. Ye, T. T. You, F. Xu, Food Hydrocoll. 137, 108355 (2023); https://doi.org/10.1016/j.foodhyd.2022.108355

[34]. D. X. Liang, X. J. Zhu, P. Dai, X. Y. Lu, H. Q. Guo, H. Que, D. D. Wang, T. He, C. Z. Xu, H. M. Robin, Z. Y. Luo, X. L. Gu , Materials Chemistry and Physics. 259, 124101 (2021); https://doi.org/10.1016/j.matchemphys.2020.124101